Nonlinear stress path experiment using mild steel sheet for validation of material model

TAKADA Yusuke[1,a] and KUWABARA Toshihiko[1,b *]

[1]Tokyo Univ. Agriculture and Technology, 2-24-16 Nakacho, Koganei-shi, Tokyo 184-8588, Japan

[a]takada.no12@gmail.com, [b]kuwabara@cc.tuat.ac.jp

Abstract. A linear stress path (LSP) experiment was performed using uniaxial and biaxial tensile tests with a cold-rolled mild steel sheet (SPCD; nominal thickness: 0.8 mm) as the test material. In the LSP experiment, nine LSPs were applied to the specimens to measure the contours of plastic work and the directions of the plastic strain rates, β, for a plastic strain range of $0.002 \leq \varepsilon_0^p \leq 0.234$. Then, the Yld2000-2d yield function (Barlat et al., 2003) was used to identify a material model that accurately reproduces the experimental data observed in the LSP experiment. Furthermore, a nonlinear stress path (NLSP) experiment was performed. The NLSP consists of two linear stress paths with $\sigma_x : \sigma_y = 4:1$ and $1:1$, and a curved stress path connecting the LSPs. The measured work hardening behavior and β values were compared with those calculated using the Yld2000-2d yield function identified from the LSP experiment. It was found that the deformation behavior of the test sample predicted by the material model determined from the LSP experiment clearly shows some deviation from that observed for the NLSP experiment.

Introduction

One of the most influential factors that affect the accuracy of sheet metal forming simulations is a material model. In order to guarantee the accuracy of the forming simulation, it is necessary to guarantee the accuracy of the material model used for the analysis. Guaranteeing the accuracy of the material model means that the deformation behavior of the material in real forming operations should be reproduced by the material model.

To experimentally determine a material model, many linear stress paths (LSPs) are applied to the material using biaxial tensile tests with cruciform test pieces [1,2] and/or the biaxial tube expansion test (BTET) with tubular specimens, to which an axial force and an internal pressure are simultaneously applied [3]. However, the stress paths in real sheet metal forming processes are generally nonlinear. Therefore, verifying that the material model determined using an LSP experiment can reproduce the deformation behavior of the material under nonlinear stress paths (NLSPs) is crucial for establishing an accurate material model.

Many studies have investigated the deformation behavior of materials subjected to NLSPs. However, most of them measured the subsequent yield surface of the materials by first applying a specific plastic strain and then, after unloading, subsequent loading paths in loading directions different from the pretrain direction to the test sample [4-8]. Of note, such NLSP experiments have been utilized to verify the validity of distortional plasticity models [9-13]. There have been several studies that have used NLSPs without unloading to verify the accuracy of material models for test samples [14-17]. However, the plastic strain applied to the test samples in these studies are less than several percent.

Takada and Kuwabara [18] investigate the deformation behavior of a cold-rolled mild steel sheet for deep drawing (SPCD) subjected to LSPs and NLSPs. The deformation behavior of the test sample is precisely measured until specimen fracture. The objective of this study is to clarify

whether the deformation behavior of a test sample under a NLSP can be reproduced using the material model determined from an LSP experiment. In this study the deviation of the NLSP from the LSP is much larger than that used in [18].

Experimental Method

The test material used in the present study was a 0.8-mm-thick mild steel sheet, SPCD, with deep drawing quality. The work hardening characteristics and *r*-values at 0°, 45°, and 90° (transverse direction, TD) with respect to the rolling direction (RD) are shown in Table 1. It is the same material as used in [18].

Table 1. Mechanical properties of test material (SPCD).

Tensile direction /°	$\sigma_{0.2}$ /MPa	ε_{TS}^{p} *	c^{**} /MPa	n^{**}	α^{**}	*r*-value***
0	146	0.241	560	0.269	0.0030	1.91
45	158	0.227	586	0.267	0.0038	1.63
90	155	0.236	563	0.271	0.0038	2.25

* Logarithmic plastic strain giving the maximum tensile load.

** Approximated using $\sigma = c(\alpha + \varepsilon^p)^n$ for $\varepsilon^p = 0.002 \sim \varepsilon_{TS}^{p}$

***Measured at uniaxial nominal strain of $\varepsilon_N = 0.1$

Two types of biaxial tensile test were performed to measure the plastic deformation behavior of the test material from initial yield to fracture. Fig. 1 (a) shows a schematic diagram of the cruciform specimen used for the biaxial tensile tests with the as-received sheet sample. The geometry of the specimen is that recommended in ISO 16842 [19]. The specimen arms were parallel to the RD and TD of the material. Each arm of the specimen had seven slits (length: 30 mm, width: 0.2 mm) at 3.75-mm intervals to remove the geometric constraint on the deformation of the 30×30 mm2 square gauge area. The slits were fabricated using laser cutting.

Fig. 1 (b) shows a schematic diagram of the tubular specimen used for the BTET. The specimens were fabricated by bending a sheet sample into a cylindrical shape and CO_2 laser welding the sheet edges together to fabricate a tubular specimen with an inner diameter of 47.1 mm, a length of 230 mm, and a gauge length (distance between the grips of the testing machine) of 150 mm. Two types of tubular specimen were fabricated. For type I specimens, the RD was in the axial direction; for type II specimens, the RD was in the circumferential direction. Type I specimens were used for the tests with $\sigma_x \leq \sigma_y$ and type II specimens were used for the tests with $\sigma_x \geq \sigma_y$; the maximum principal stress direction was always taken to be the circumferential direction. Because the measurement results for the BTET include the effect of prestrain due to bending during the preparation of the circular tube test pieces, they were corrected using the data obtained from the cruciform test piece. For details, refer to [3].
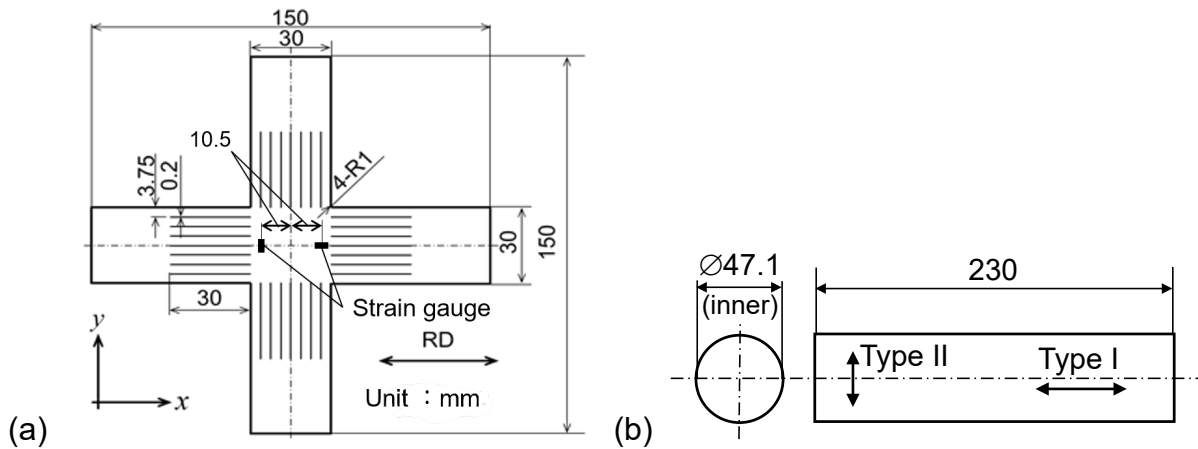
Fig. 1. Specimens used for biaxial tensile tests [19]. (a) Cruciform specimen and (b) tubular specimen. In (b), ↔ indicates the RD of the original sheet sample. The RD is taken in the axial direction for type I specimens and in the circumferential direction for type II specimens.

For details of the servo-controlled tension-internal pressure testing machine used in the experiment, see [3]. For details of the measurement method of the axial and circumferential strain components, ε_ϕ and ε_θ, the axial radius of curvature, R_ϕ, and the calculation method of the axial and circumferential stress components, σ_ϕ and σ_θ, see [20].

Linear Stress Path Experiment. For the LSP experiment, both cruciform and tubular specimens were subjected to seven LSPs, namely $\sigma_x:\sigma_y$ = 4:1, 2:1, 4:3, 1:1, 1:2, 3:4, and 1:4, where σ_x and σ_y are the true stress in the RD and TD, respectively. For $\sigma_x:\sigma_y$ =1:0 and 0:1, the uniaxial tensile test specimens standardized in JIS13B were used. The equivalent plastic strain rate was controlled to be approximately constant at $5 \times 10^{-4}\ \mathrm{s}^{-1}$.

Nonlinear Stress Path Experiment. Fig. 2 shows the NLSP applied to the test sample in the NLSP experiment. The NLSP was determined by assuming that the material deforms following the IH model based on the Yld2000-2d yield function [21] as determined in Fig. 3. The first stress path was the LSP with $\sigma_x:\sigma_y = 4:1$. When ε_0^p reached 0.07, the stress path was changed to the second loading. ε_0^p gradually increased along the second loading. Then, when ε_0^p reached 0.09, the stress path followed the LSP with $\sigma_x:\sigma_y$ =1:1. The equivalent plastic strain rate was controlled to be approximately constant at $5 \times 10^{-4}\ \mathrm{s}^{-1}$. Two specimens, Exp.1 and Exp.2, were used for the NLSP experiment.
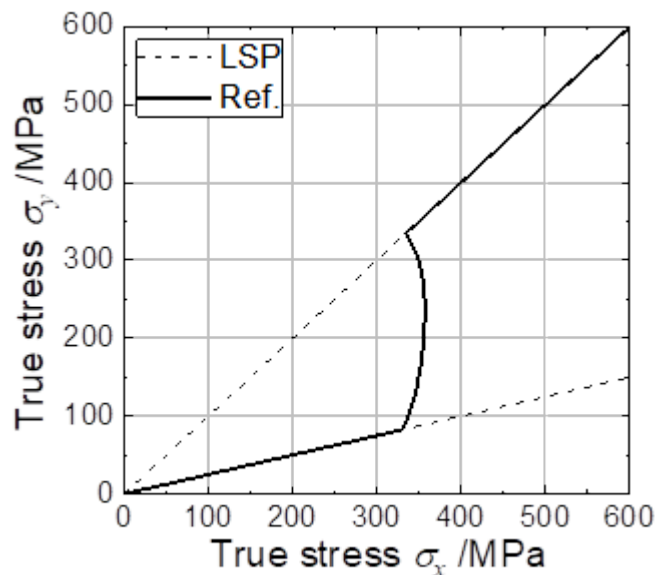

Fig. 2. Nonlinear stress path.

In the NLSP experiment, the evolution of $\varepsilon_x^p(t)$ and $\varepsilon_y^p(t)$ was approximated using a polynomial function for every stress path section between abrupt stress path change points, and the instantaneous value of β was calculated as $\tan^{-1}\{d\varepsilon_y^p(t)/d\varepsilon_x^p(t)\}$.

Experimental Results

The contours of plastic work in the stress space [22,23] were measured to identify appropriate material models for the test samples subjected to uniaxial and biaxial tension. With the true stress-logarithmic plastic strain curve measured for the RD used as reference data for work hardening, the plastic work per unit volume, W_0, and uniaxial true stress, σ_0, associated with particular values of ε_0^p (referred to as the reference plastic strain hereafter) were determined. Next, from the biaxial and uniaxial stress-strain curves, the stress points that give the same plastic work as W_0 were plotted in the principal stress space to determine the contour of plastic work associated with ε_0^p.

Fig. 3 shows the stress points that form work contours. Each stress point represents an average of two specimen data points; the difference between the two points was less than 1.4% of the flow stress for all data points. We measured up to $\varepsilon_0^p = 0.234$ for all LSPs. To quantitatively evaluate the shape change of the work contours with increasing ε_0^p, the nondimensional work contours were determined by dividing the value of the stress points that formed each work contour by the σ_0 value belonging to the work contour. It was confirmed that the stress points along the stress paths of $\sigma_x:\sigma_y = 4:1$, 2:1, 4:3, 1:1, and 3:4 do not fall on a single point with increasing ε_0^p; therefore, the test material exhibited differential hardening (DH). Fig. 3 also includes the yield loci calculated using the selected yield functions. The solid line is that based on the Yld2000-2d yield function, the exponent, M, and parameters, $\alpha_1 - \alpha_6$, of which were determined to approximate the shape of the work contour and the directions of the plastic strain rate, D^p, for $\varepsilon_0^p = 0.10$. The evolution of the work contours with ε_0^p is well reproduced by the DH model based on the Yld2000-2d yield function, as indicated by the red and black dotted lines for $\varepsilon_0^p = 0.002$ and 0.10, respectively.
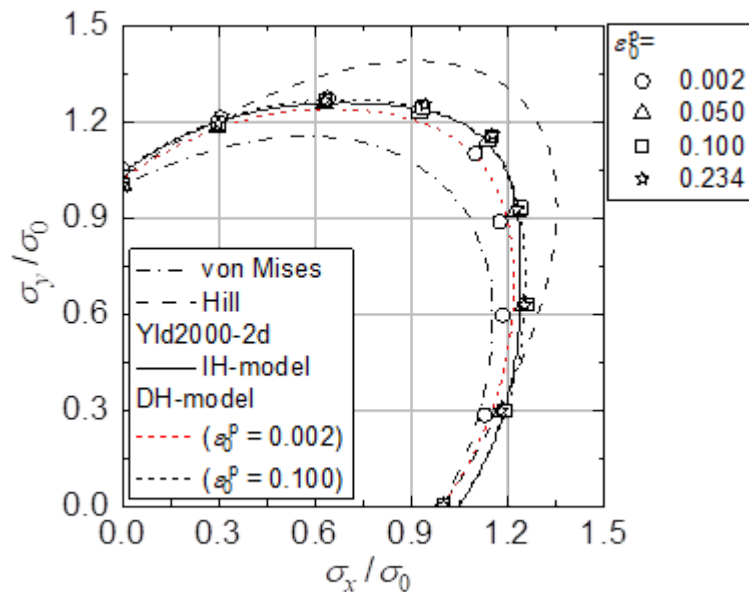

Fig. 3. Measured contours of plastic work normalized by σ_0 belonging to same group of work contours.

Fig. 4 compares the measured directions of D^p, β, with those predicted using the selected yield functions. Again, the measured data are well reproduced by the Yld2000-2d yield function for all loading directions. Moreover, it is noteworthy that the experimental tendency for β to decrease for $\sigma_x:\sigma_y = 4:3$ and increase for $\sigma_x:\sigma_y = 3:4$ with increasing ε_0^p was well reproduced by the DH model.

In summary, the evolution of the contours of plastic work and the directions of the plastic strain rates with increasing ε_0^p measured in the LSP experiment are accurately reproduced by the DH model based on the Yld2000-2d yield function.
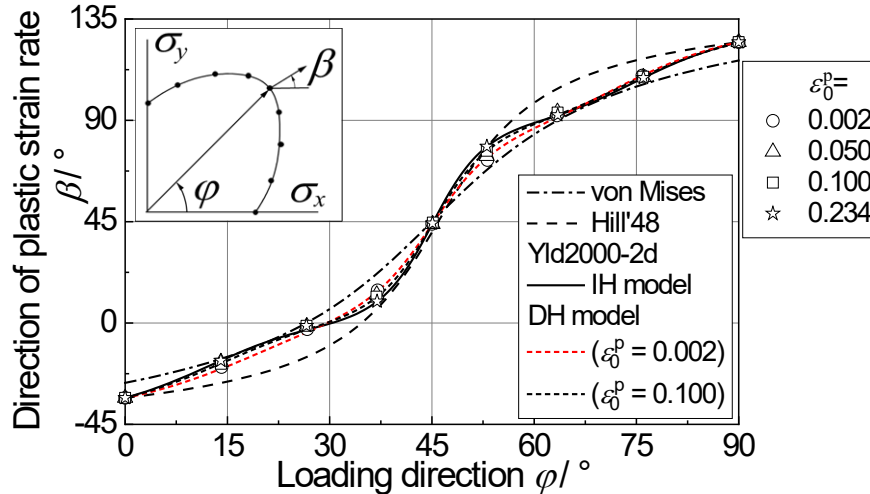
Fig. 4. Measured directions of plastic strain rates compared with those calculated using selected yield functions.

Fig. 5 shows the $\sigma_x - \varepsilon_x^{\mathrm{p}}$ and $\sigma_y - \varepsilon_y^{\mathrm{p}}$ curves observed for the NLSP shown in Fig. 2. Two specimens were used, and the reproducibility of the two tests was good. The small protrusion in the black line was caused by the change in σ_x along the second (curved) stress path.
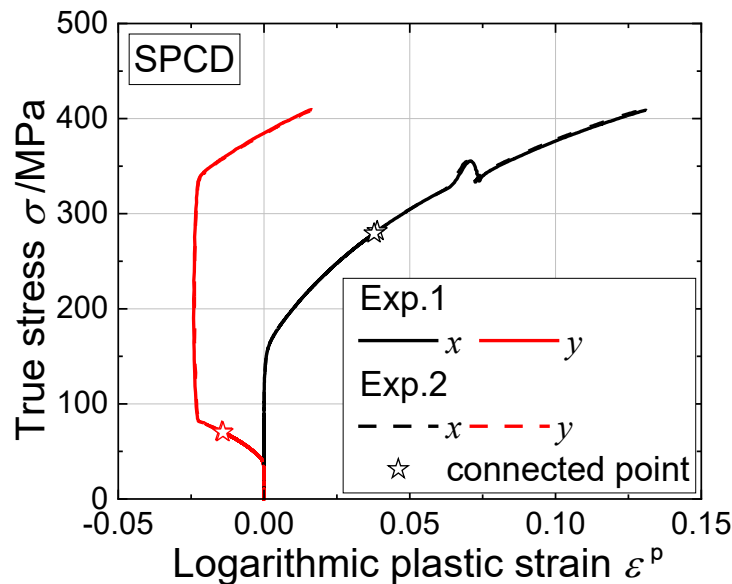

Fig. 5. $\sigma_x - \varepsilon_x^p$ and $\sigma_y - \varepsilon_y^p$ curves observed for the NLSP shown in Fig. 2. Those for the lower strain range than the star marks were measured using a cruciform specimen, and those for the higher strain range than the star marks were measured using the BTET.

Fig. 6 shows the variation of loading direction, φ, with increasing $\varepsilon_0^{\mathrm{p}}$ for the stress path shown in Fig. 2. The largest deviation of the experimental values from the prediction by the Yld2000-2d yield function with DH was $\Delta\varphi = 5.8°$ at $\varepsilon_0^{\mathrm{p}} = 0.08$.
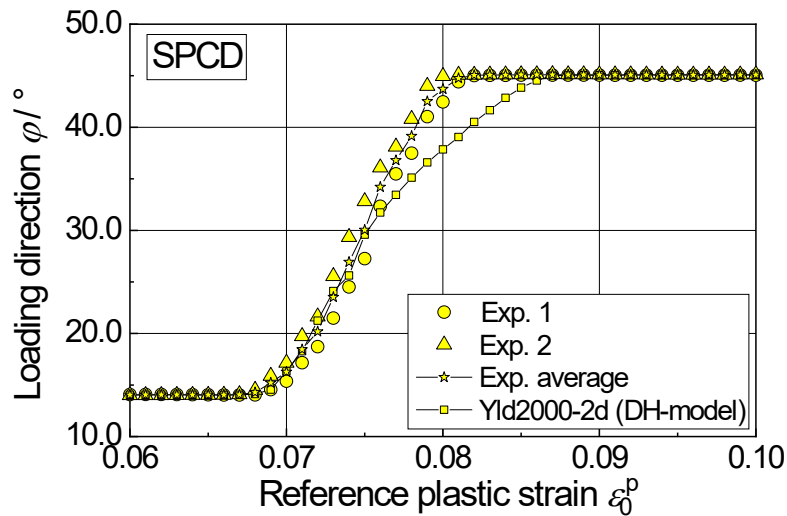
Fig. 6. Variation of loading direction, φ, with increasing ε_0^p for the stress path shown in Fig. 2.

Fig. 7 shows the change in the direction of plastic strain rate, β, with increasing ε_0^p for the stress path shown in Fig. 2. The largest deviation of the experimental values from the prediction by the Yld2000-2d yield function with DH was $\Delta\beta = 20.4°$ at $\varepsilon_0^p = 0.08$. It is noted that β reached 35° at $\varepsilon_0^p = 0.08$, and remained almost constant at $\beta = 35°$ for $\varepsilon_0^p \geq 0.08$; it was 9° lower than the prediction by the Yld2000-2d yield function. Considering that the stress state almost reached equibiaxial tension at $\varepsilon_0^p = 0.08$ in the experiment, this difference in β between the NLSP and LSP was possibly caused by the change in texture during the NLSP for $\varepsilon_0^p \leq 0.08$. Therefore, we can conclude that the deformation behavior predicted by the material model determined from the LSP experiment clearly shows some deviation from that observed for the NLSP experiment.
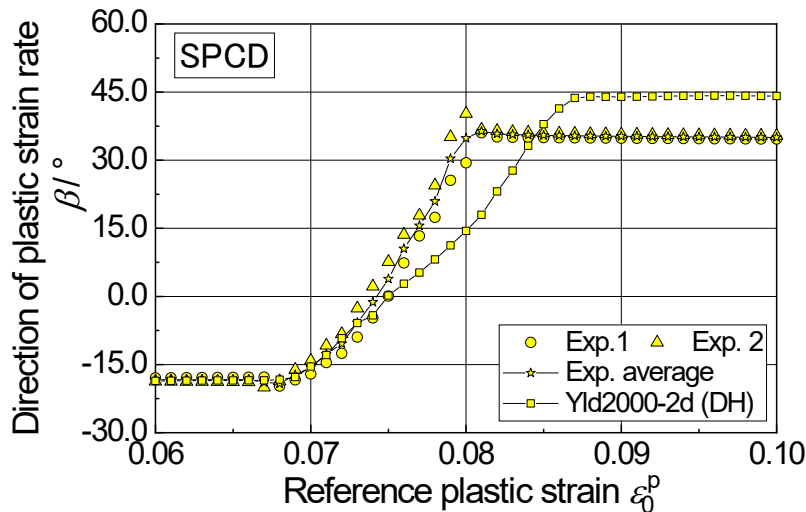

Fig. 7. Change in direction of plastic strain rate, β, with increasing ε_0^p for the stress path shown in Fig. 2.

Summary
The deformation behavior of a mild steel sheet was observed both for the LSPs and NLSP. A proper material model was determined from the LSP experiment using the Yld2000-2d yield

function. Moreover, a NLSP experiment was performed for the test sample, and the deformation behavior of the test sample during the NLSP experiment was precisely measured, and compared with that predicted using the Yld2000-2d yield function. It was found that the deformation behavior of the test sample predicted by the material model determined from the LSP experiment clearly shows some deviation from that observed for the NLSP experiment.

References

[1] T. Kuwabara, S. Ikeda, K. Kuroda, Measurement and analysis of differential work-hardening in cold-rolled steel sheet under biaxial tension, J. Mater. Process. Technol. 80-81 (1998) 517-523. https://doi.org/10.1016/S0924-0136(98)00155-1

[2] T. Kuwabara, A. Van Bael, E. Iizuka, Measurement and analysis of yield locus and work-hardening characteristics of steel sheets with different R-values, Acta Mater. 50 (2002) 3717-3729. https://doi.org/10.1016/S1359-6454(02)00184-2

[3] T. Kuwabara, F. Sugawara, Multiaxial tube expansion test method for measurement of sheet metal deformation behavior under biaxial tension for a large strain range. Int. J. Plast. 45 (2013) 103-118. http://doi.org/10.1016/j.ijplas.2012.12.003

[4] S.S. Hecker, Yield surfaces in prestrained aluminum and copper, Metal. Trans. 2 (1971) 2077-2086. https://doi.org/10.1007/BF02917534

[5] K. Ikegami, A historical perspective of experimental study on subsequent yield surfaces for metals (part 1), J. Soc. Mat. Sci., Jpn. 24 (1975) 491-504 (in Japanese) https://doi.org/10.2472/jsms.24.491

[6] K. Ikegami, A historical perspective of experimental study on subsequent yield surfaces for metals (part 2), J. Soc. Mat. Sci., Jpn., 24 (1975) 709-719 (in Japanese). https://doi.org/10.2472/jsms.24.709

[7] Y. Ohashi, K. Kawashima, T. Yokochi, Anisotropy due to plastic deformation of initially isotropic mild steel and its analytical formulation, J. Mech. Phys. Solid. 23 (1975) 277-294. https://doi.org/10.1016/0022-5096(75)90029-0

[8] E. Shiratori, K. Ikegami, K. Kaneko, The influence of the Bauschinger effect on the subsequent yield condition, Bull. JSME 16 (1973) 1482-1493. https://doi.org/10.1299/jsme1958.16.1482

[9] F. Barlat, S.Y. Yoon, S.Y. Lee, M.S. Wi, J.H. Kim, Distortional plasticity framework with application to advanced high strength steel, Int. J. Solids Struct. 202 (2020) 947-962. https://doi.org/10.1016/j.ijsolstr.2020.05.014

[10] J.J. Ha, M.-G. Lee, F. Barlat, Strain hardening response and modeling of EDDQ and DP780 steel sheet under non-linear strain path, Mech. Mater. 64 (2013) 11-26. http://dx.doi.org/10.1016/j.mechmat.2013.04.004

[11] H. Kim, F. Barlat, Y. Lee, S.B. Zaman, C.S. Lee, Y. Jeong, A crystal plasticity model for describing the anisotropic hardening behavior of steel sheets during strain-path changes, Int. J. Plast. 111 (2018) 85-106. https://doi.org/10.1016/j.ijplas.2018.07.010

[12] J. Qin, B. Holmedal, O.S. Hopperstad, A combined isotropic, kinematic and distortional hardening model for aluminum and steels under complex strain-path changes, Int. J. Plast. 101 (2018) 156-169. https://doi.org/10.1016/j.ijplas.2017.10.013

[13] M.S. Wi, S.Y. Lee, J.H. Kim, J.M. Kim, F. Barlat, Experimental and theoretical plasticity analyses of steel materials deformed under a nonlinear strain path, Int. J. Mech. Sci. 182 (2020) 105770. https://doi.org/10.1016/j.ijmecsci.2020.105770

[14] S.S. Hecker, Experimental Investigation of Corners in the Yield Surface, Acta Mech. 13 (1972) 69-86. https://doi.org/10.1007/BF01179659

[15] T. Kuwabara, M. Kuroda, V. Tvergaard, K. Nomura, Use of abrupt strain path change for determining subsequent yield surface: experimental study with metal sheets, Acta Mater. 48 (2000) 2071-2079. https://doi.org/10.1016/S1359-6454(00)00048-3

[16] K. Yoshida, T. Tsuchimoto, Plastic flow of thin-walled tubes under nonlinear tension-torsion loading paths and an improved pseudo-corner model, Int. J. Plast. 104 (2018) 214-229. https://doi.org/10.1016/j.ijplas.2018.02.013

[17] T. Hama, S. Yagi, K. Tatsukawa, Y. Maeda, Y. Maeda, H. Takuda, Evolution of plastic deformation behavior upon strain-path changes in an A6022-T4 Al alloy sheet, Int. J. Plast. 137 (2021) 102913. https://doi.org/10.1016/j.ijplas.2020.102913

[18] Y. Takada, T. Kuwabara, Nonlinear biaxial tensile stress path experiment without intermediate elastic unloading for validation of material model, Int. J. Solid. Struct. 257 (2022) 111777. https://doi.org/10.1016/j.ijsolstr.2022.111777

[19] ISO 16842: 2014 Metallic materials −Sheet and strip −Biaxial tensile testing method using a cruciform test piece.

[20] T. Hakoyama, T. Kuwabara, Effect of biaxial work hardening modeling for sheet metals on the accuracy of forming limit analyses using the Marciniak-Kuczynski approach, in: H. Altenbach, T. Matsuda, D. Okumura (Eds.), From Creep Damage Mechanics to Homogenization Methods, Springer, 2015, pp. 67-95. https://doi.org/10.1007/978-3-319-19440-0_4

[21] F. Barlat, J.C. Brem, J.W. Yoon, K. Chung, R.E. Dick, D.J. Lege, F. Pourboghrat, S.H. Choi, E. Chu, Plane stress yield function for aluminum alloy sheets-part 1: theory, Int. J. Plast. 19 (2003) 1297-1319. https://doi.org/10.1016/S0749-6419(02)00019-0

[22] R. Hill, J.W. Hutchinson, Differential hardening in sheet metal under biaxial loading: a theoretical framework, J. Appl. Mech. 59 (1992) S1-S9. https://doi.org/10.1115/1.2899489

[23] R. Hill, S.S. Hecker, M.G. Stout, An investigation of plastic flow and differential work hardening in orthotropic brass tubes under fluid pressure and axial load, Int. J. Solid. Struct. 31 (1994) 2999-3021. https://doi.org/10.1016/0020-7683(94)90065-5